

Measurement of charm production in neutrino charged-current interactions

CHORUS Collaboration

July 3, 2013

Abstract

The nuclear emulsion target of the CHORUS detector was exposed to the wide-band neutrino beam of the CERN SPS of 27 GeV average neutrino energy from 1994 to 1997. In total about 100000 charged-current neutrino interactions with at least one identified muon were located in the emulsion target and fully reconstructed, using newly developed automated scanning systems. Charmed particles were searched for by a program recognizing particle decays. The observation of the decay in nuclear emulsion makes it possible to select a sample with very low background and minimal kinematical bias. 2013 charged-current interactions with a charmed hadron candidate in the final state were selected and confirmed through visual inspection. The charm production rate induced by neutrinos relative to the charged-current cross-section is measured to be $\sigma(\nu_\mu N \rightarrow \mu^- CX)/\sigma(CC) = (5.75 \pm 0.32(\text{stat}) \pm 0.30(\text{syst}))\%$. The charm production cross-section as a function of the neutrino energy is also obtained. The results are in good agreement with previous measurements. The charm-quark hadronization produces the following charmed hadrons with relative fractions (in %): $f_{D^0} = 43.7 \pm 4.5$, $f_{\Lambda_c^+} = 19.2 \pm 4.2$, $f_{D^+} = 25.3 \pm 4.2$, and $f_{D_s^+} = 11.8 \pm 4.7$.

CHORUS Collaboration

A. Kayis-Topaksu, G. Öngüt
Çukurova University, Adana, Turkey

R. van Dantzig, M. de Jong, R.G.C. Oldeman¹
NIKHEF, Amsterdam, The Netherlands

M. Güler, U. Köse, P. Tolun
METU, Ankara, Turkey

M.G. Catanesi, M.T. Muciaccia
Università di Bari and INFN, Bari, Italy

K. Winter
Humboldt Universität, Berlin, Germany²

B. Van de Vyver³, P. Vilain⁴, G. Wilquet⁴
Inter-University Institute for High Energies (ULB-VUB) Brussels, Belgium

B. Saitta
Università di Cagliari and INFN, Cagliari, Italy

E. Di Capua
Università di Ferrara and INFN, Ferrara, Italy

S. Ogawa, H. Shibuya
Toho University, Funabashi, Japan

I.R. Hristova⁵, T. Kawamura, D. Kolev⁶, H. Meinhard, J. Panman, A. Rozanov⁷, R. Tsenov⁶,
J.W.E. Uiterwijk, P. Zucchelli⁸
CERN, Geneva, Switzerland

J. Goldberg
Technion, Haifa, Israel

M. Chikawa
Kinki University, Higashioaka, Japan

J.S. Song, C.S. Yoon
Gyeongsang National University, Jinju, Korea

K. Kodama, N. Ushida
Aichi University of Education, Kariya, Japan

S. Aoki, T. Hara
Kobe University, Kobe, Japan

T. Delbar, D. Favart, G. Grégoire, S. Kalinin, I. Makhlioueva
Université Catholique de Louvain, Louvain-la-Neuve, Belgium

A. Artamonov, P. Gorbunov, V. Khovansky, V. Shamanov, I. Tsukerman
Institute for Theoretical and Experimental Physics, Moscow, Russian Federation

N. Bruski, D. Frekers
Westfälische Wilhelms-Universität, Münster, Germany²

K. Hoshino, J. Kawada⁹, M. Komatsu, M. Miyanishi, M. Nakamura, T. Nakano, K. Narita, K. Niu,
K. Niwa, N. Nonaka, O. Sato, T. Toshito

Nagoya University, Nagoya, Japan

S. Buontempo, A.G. Cocco, N. D'Ambrosio, G. De Lellis, G. De Rosa, F. Di Capua*, G. Fiorillo,
A. Marotta, M. Messina, P. Migliozzi, L. Scotto Lavina, P. Strolin, V. Tioukov

Università Federico II and INFN, Naples, Italy

T. Okusawa

Osaka City University, Osaka, Japan

U. Dore, P.F. Loverre, L. Ludovici, G. Rosa, R. Santacesaria, A. Satta, F.R. Spada

Università La Sapienza and INFN, Rome, Italy

E. Barbuto, C. Bozza, G. Grella, G. Romano, C. Sirignano, S. Sorrentino

Università di Salerno and INFN, Salerno, Italy

Y. Sato, I. Tezuka

Utsunomiya University, Utsunomiya, Japan

¹ now at Università di Cagliari and INFN, Cagliari, Italy.

² Supported by the German Bundesministerium für Bildung und Forschung under contract numbers 05 6BU11P and 05 7MS12P.

³ Fonds voor Wetenschappelijk Onderzoek, Belgium.

⁴ Fonds National de la Recherche Scientifique, Belgium.

⁵ Now at DESY, Hamburg.

⁶ On leave of absence and at St. Kliment Ohridski University of Sofia, Bulgaria.

⁷ Now at CPPM CNRS-IN2P3, Marseille, France.

⁸ On leave of absence from INFN, Ferrara, Italy.

⁹ Now at University of Bern, Switzerland.

* Corresponding author, email: dicapua@na.infn.it

1 Physics motivation

About forty years after the discovery of the charm quark at SLAC [1] and BNL [2], and the first observation of charm decay in nuclear emulsion [3], the study of the charmed particles is still a challenging field of particle physics. In particular, the neutrino induced charm-production offers the possibility to study the strange-quark content of the nucleon, to measure “directly” the CKM matrix element V_{cd} and to test models for charm-production and subsequent hadronization. Moreover, neutrinos produce charmed hadrons also via specific processes like quasi-elastic and diffractive scattering which provide a unique tool for studies of exclusive charm production.

In addition to its intrinsic interest, an improved knowledge of charm production helps to better understand the charm background in neutrino oscillation experiments where the signal is given by the production of a τ lepton or of muons of apparently “wrong” charge with respect to that expected from the neutrino beam helicity, as in ongoing experiments [4] and at future neutrino facilities [5].

Charm production in neutrino and anti-neutrino charged-current (CC) interactions has been studied by several experiments by looking at the presence of two oppositely charged leptons in the final state. In particular, CDHS [6], CCFR [7], CHARM [8], CHARM-II [9], NuTeV [10] and CHORUS (using only its electronic detectors) [11] have collected large statistics of opposite-sign dimuon events. The leading muon is interpreted as originating from the neutrino vertex and the other one, of opposite charge, as being the decay product of the charmed particle. Although massive electronic detectors allow obtaining large statistics, they have some drawbacks. Of the charmed parent only the decay muon is seen, resulting in an event sample composed of a mixture of all charmed-particle species weighted by their muonic branching ratios. Furthermore, experiments of this type suffer from significant background ($\sim 20\%$) due to the undetected decay-in-flight of a pion or a kaon. The identification of the primary muon and the decay muon is not unambiguous. Moreover the kinematic cuts on the energies of the primary and decay muons, required for background reduction, make it difficult to study cross-sections at energies below 20–30 GeV.

Unlike dimuon experiments, BEBC [12] and NOMAD [13] were able to recognize specific charm decay modes by reconstructing an invariant mass from the decay daughters. Only a few specific decay modes were selected and thus also a specific parent particle type. CHORUS [14] took advantage of the spatial resolution of nuclear emulsion to distinguish the charm decay vertex from the primary neutrino interaction vertex. In combination with a measurement of the transverse momentum of one of the decay products it could select a specific decay mode of the D^{*+} with very low background.

The use of a hybrid nuclear emulsion detector was pioneered by the E531 [15] experiment at FNAL. In nuclear emulsion, the different charmed particles are recognized on the basis of their decay topology and short flight length, so that the required kinematic cuts can be quite loose. All decay channels are therefore observed, not only the muonic ones, without requiring knowledge of muonic branching ratios and with very low background. The disadvantage of the low statistics generally obtained in emulsion experiments (122 charm events observed in E531) has been overcome in the CHORUS experiment [16] by using a massive (770 kg) nuclear emulsion target and automated emulsion scanning [17, 18]. A high-statistics sample of charm decays in emulsion, more than one order of magnitude larger than in E531, has thus been collected as reported in this paper.

The CHORUS experiment took data from 1994 to 1997 in the CERN Wide Band Neutrino Beam [19] which essentially consisted of muon neutrinos. The analysis presented here is based on the complete CHORUS sample of 2013 charm events, confirmed by visual inspection. The visual inspection recognized 1048 events as due to the production of the neutral charmed hadron D^0 and 965 events as due to the production

of a charged charmed hadron Λ_c^+ , D^+ or D_s^+ . The analysis of the D^0 events has been reported in a previous publication [20]. The charged sample is analysed in this paper. The relative contribution of the different charmed hadrons to the total charged sample is obtained from a likelihood approach by using the decay lifetime information.

The neutral and charged charm production candidates are combined for the measurement of the total charm production rate relative to charged-current neutrino events averaged on the neutrino energy spectrum as well as of its dependence on neutrino energy.

2 The experimental set-up

The CHORUS experiment was designed to investigate neutrino oscillation by searching for the ν_τ appearance in the SPS wide-band neutrino beam at CERN through the direct observation of the τ decay in nuclear emulsions. Since charmed particles have a flight length comparable to that of the τ lepton, the experiment is also suitable for the study of charm production. The detector, described in more detail in [16], uses a hybrid approach that combines a nuclear emulsion target with electronic detectors.

The emulsion target, of 770 kg total mass, is segmented along the beam direction in four stacks of $1.4 \times 1.4 \text{ m}^2$ transverse area and about 3 cm thickness. It is equipped with high-resolution trackers made out of three interface emulsion sheets and a set of scintillating fibre tracker planes which provides predictions of particle trajectories into the emulsion stack with an accuracy of about $150 \text{ }\mu\text{m}$ in position and 2 mrad in angle.

The emulsion scanning is performed by computer-controlled, fully automated microscope stages equipped with a CCD camera and a read-out system called ‘track selector’ [17, 18]. The track-finding efficiency is higher than 98% for track slopes up to 400 mrad.

The electronic detectors downstream of the emulsion target include a hadron spectrometer, a calorimeter and a muon spectrometer. The hadron spectrometer measures the bending of charged particles inside an air-core magnet. The calorimeter is used to determine the energy and direction of showers. The muon spectrometer provides the charge and momentum of muons and provides a rough measurement of the leakage of hadronic showers out of the calorimeter. Several planes of scintillator hodoscopes are used for triggering the data acquisition system [21].

3 Data collection

The CHORUS detector was exposed to the wide-band neutrino beam of the CERN SPS during the years 1994–97, with an integrated flux of 5.06×10^{19} protons on target. The beam, of 27 GeV average energy, consists mainly of ν_μ ’s with a 5% $\bar{\nu}_\mu$ component of 18 GeV average energy.

The series of steps in the location process of a CC event starts with the track reconstruction in the electronic detectors, including the muon identification and terminates with the association to the primary and possibly secondary vertices of the tracks recorded in a volume of emulsion. The event location process is summarized in [20] and detailed in [22] and [23]. The so-called ‘NetScan’ method used to analyse the emulsion volume around the interaction point is described in [22] and [24].

About 150 000 events have been located in the emulsion target and have been analysed following this procedure.

Table 1: Charged-current data sample and charm candidates.

Located CC events	93807
Selected for visual inspection	2752
Decay topologies with flight length $< 25 \mu\text{m}$	3
Topologies with kink angle $< 50 \text{ mrad}$	11
Secondary interactions	278
Electron–positron pairs	95
Overlaid neutrino interactions	44
Uncorrelated (overlaid) secondary vertices	21
Passing-through tracks	128
All tracks from primary vertex	142
δ -rays	2
Other	15
Charged charm candidates	965
C1	452
C3	491
C5	22
Neutral charm candidates	1048
V2	819
V4	226
V6	3
Total charm candidates	2013

An event is recognized as a charged-current neutrino interaction if the primary muon track, defined by the electronic detectors, is found in more than one emulsion plate. Decay topologies are selected using the following criteria. At least one of the tracks connected to a secondary vertex is detected in more than one plate, and the direction measured in the emulsion matches that of a track reconstructed in the fibre tracker system. The parent angle is within 400 mrad from the beam direction. In the case of a neutral particle decay, the parent angle is deduced from the line connecting the primary and secondary vertex. The impact parameter to the primary vertex of at least one of the daughter tracks is larger than a value which is determined on the basis of the resolution¹. To remove random association, the impact parameter is also required to be smaller than a value depending on the distance over which the track is extrapolated to the vertex, typically of the order of 130 μm . The flight length of the parent candidate is required to be larger than 25 μm .

Out of a sample of 143742 located neutrino-induced charged-current interaction vertices, 93807 were fully scanned and analysed. The selection criteria retain 2752 events as having a decay topology. These have all been visually inspected. The presence of a decay was confirmed for 2013 events. A secondary vertex is accepted as a decay if the number of charged particles is consistent with charge conservation and no other activity (Auger-electron or visible recoil) is observed. The purity of the automatic selection is 73.2%.

¹The resolution to extrapolate to the vertex depends on the track angle θ with respect to the beam according to the relation $\sigma = \sqrt{0.003^2 + (0.0194 \cdot \tan \theta)^2}$ mm.

The result of the visual inspection is given in Table 1 where according to the prong multiplicity the observable decay topologies are classified as even-prong decays V2, V4 or V6 for neutral particles (mainly D^0) and odd-prong decays C1, C3 or C5 for charged particles (mainly Λ_c^+ , D^+ , D_s^+). The rejected sample consists of secondary hadronic interactions, δ -rays or gamma conversions, overlaid neutrino interactions, and of low-momentum tracks which, because of multiple scattering appear as tracks with a large impact parameter. The remainder consists either of fake vertices, being reconstructed using one or more background tracks, or of vertices with a parent track not connected to the primary (passing-through tracks not identified as such because of inefficiencies).

As shown in Table 1 we find 965 charged charm candidates (452 with C1 topology, 491 with C3 and 22 with C5) and 1048 neutral charm candidates (819 with V2 topology, 226 with V4 and 3 with V6).

4 Reconstruction efficiency and background evaluation

The efficiency of the event reconstruction in the electronic detector as well as those of the event location and reconstruction in the emulsion, need to be evaluated.

When the neutrino scatters off a nucleon, several physical mechanisms produce charmed hadrons. However, they are predominantly produced in deep-inelastic interactions. Different Monte Carlo generators are used [25]. The neutrino beam spectrum is simulated using the GBEAM [26] generator based on GEANT3 [27]. It uses FLUKA98 [28] to describe the interactions of protons with the beryllium target.

Deep-inelastic scattering interactions are simulated using the JETTA generator [29] which is based on LEPTO 6.1 [30] and JETSET [31]. This generator is used to simulate charm-production as well as inclusive CC interactions. Quasi-elastic interactions and resonance production processes are simulated with the RESQUE generator [32]. In addition, some other charm-production mechanisms are simulated: quasi-elastic charmed baryon production by QEGEN [33] and diffractive production of charmed mesons by the ASTRA generator [34].

The simulation of the detector response as well as the performance of the pattern recognition in the electronic tracking detectors is performed for each process by a GEANT3 [27] based simulation program. The simulated response of the electronic detectors is processed through the same analysis chain as the raw data obtained with the detector. The event location technique in emulsion is parametrized by a function of the primary muon momentum and angle, taking into account that the muon momentum distribution is different for the two samples of CC events containing charm or not.

To evaluate the efficiency to reconstruct decay topologies of the charmed hadrons, realistic conditions of track densities in the emulsion have to be reproduced. These are obtained by merging the emulsion data of simulated events with real NetScan data which do not have a reconstructed vertex but contain tracks which stop or pass through the NetScan fiducial volume. These so-called ‘empty volumes’ represent a realistic background. The combined data are passed through the same NetScan reconstruction and selection programs as used for real data. The details of the response of the automatic microscopes are used in this calculation. Important parameters are the angular resolution and efficiency as function of the incident angle of the track.

To evaluate the detection efficiency for charmed hadrons, the branching ratios and the corresponding uncertainties are taken into account. The contribution from QE and DIS interactions to the production of charmed baryons is evaluated as discussed in [35]. The contribution of diffractive charm production is evaluated by using the method described in [36]. The D^0 detection efficiency is given in [20]. Only

Table 2: Overall selection efficiency relative to CC containing geometrical acceptance and reconstruction efficiency for charged charmed hadrons decaying into one, three and five prongs, respectively.

	Λ_c^+	D^+	D_s^+
$C^+ \rightarrow 1p$ (%)	17.1 ± 1.3	21.7 ± 0.9	23.9 ± 1.2
$C^+ \rightarrow 3p$ (%)	40.8 ± 1.6	49.0 ± 1.2	57.7 ± 1.4
$C^+ \rightarrow 5p$ (%)	44.2 ± 5.2	52.7 ± 6.5	57.3 ± 3.4
$\epsilon_{3p}/\epsilon_{1p}$	2.3 ± 0.2	2.3 ± 0.1	2.4 ± 0.1

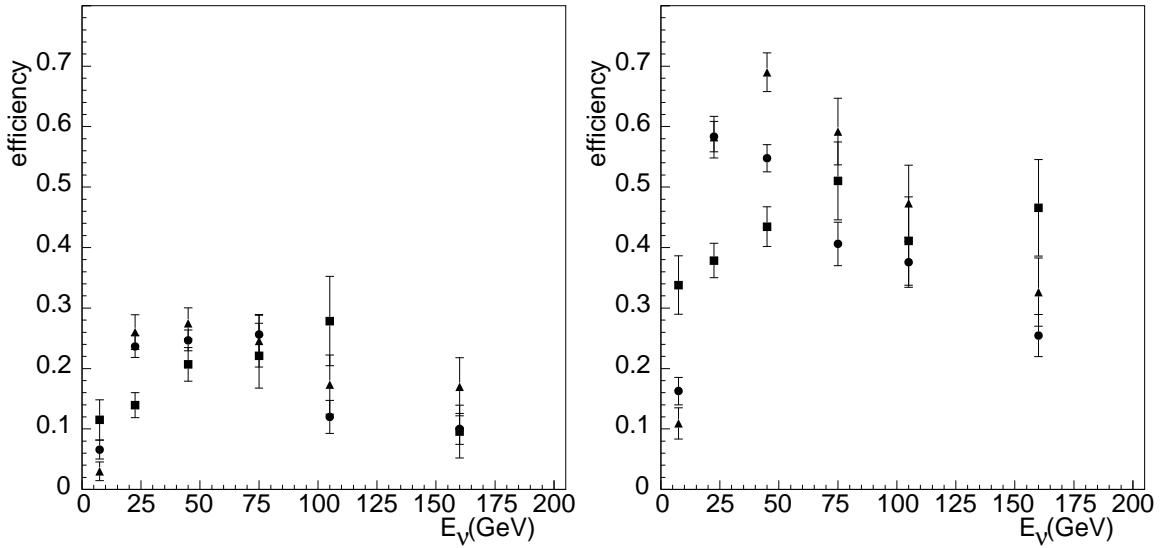


Figure 1: Detection efficiency of charged charm hadrons relative to CC interactions as a function of neutrino energy for 1-prong decay (left panel) and 3-prong decays (right panel). The data points indicated with circles show the efficiency for D^+ detection, the points marked with triangles are for D_s^+ detection and squares for Λ_c^+ .

ratios of the electronic reconstruction and vertex location efficiencies need to be determined, thus reducing significantly the systematic error. The overall selection efficiencies relative to the selection of CC events for different decay topologies are shown in Table 2. The requirement that at least one track of the secondary vertex be matched with a track in the electronic detectors causes the efficiency to be higher with increasing number of prongs at the decay vertex.

Figure 1 shows the detection efficiency of charged charmed hadrons D^+ , D_s^+ and Λ_c^+ relative to CC interactions as a function of neutrino energy. Two factors make the selection less efficient at small visible energies: the decay angle of the charm daughters is larger; the flight length of the charm parent is shorter and thus a secondary track might be wrongly attached to the primary vertex. At high energies, a large fraction of charmed hadron decays near the edge or beyond the fiducial volume.

The spread in the performance of the microscopes is found to induce a difference of $\pm 2\%$ in the calculation of the selection efficiencies for the charm detection. The weighted average performance of the individual microscope stages is taken for the calculation in order to minimize the uncertainty. The uncer-

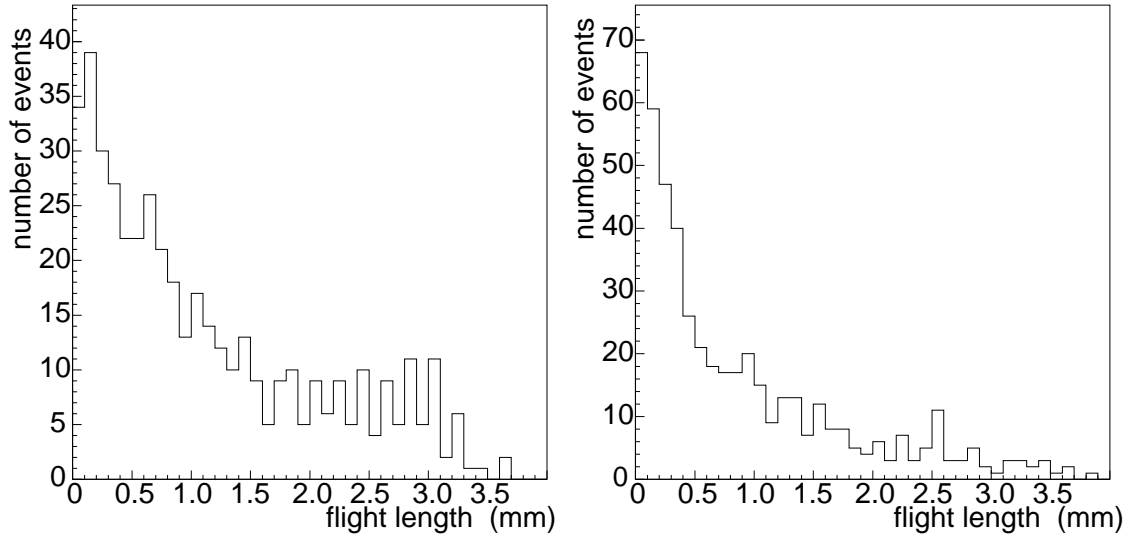


Figure 2: The flight length distributions for the 1-prong (left) and 3-prong (right) charged charm events. The distributions are truncated due to the limited NetScan volume.

tainty on the efficiency combination of several charm production mechanisms introduces an additional error on the efficiency of $\pm 12\%$ for Λ_c^+ and $\pm 3\%$ for D_s^+ . Including also other factors, such as the uncertainty in the fragmentation, we estimate a total systematic uncertainty in the efficiency of 14% for Λ_c^+ , 5% for D^+ and 6% for D_s^+ relative to CC event detection.

There is a small fraction of non-charm events in the manually confirmed sample. This contamination is mainly due to hadronic interactions with no heavily ionizing tracks or other evidence for nuclear break-up (blobs or Auger electrons) that fake charm decays (white kinks) and decays of Σ^\pm , K_s^0 and Λ^0 . The backgrounds from the decays of strange particles were estimated using the JETTA [29] MC generator.

In the D^0 sample, the strange-particle decay background has been evaluated to be $11.5 \pm 1.9 \Lambda^0$'s and $25.1 \pm 2.9 K_s^0$'s in the V2 sample and negligible for the other D^0 decay topologies [20]. For charged charmed hadrons, the expected background in the C1 sample from the decay of charged strange particles is 8.5 ± 1.3 events.

The background due to white kink interactions is obtained by generating such kind of interactions assuming a hadron interaction length $\lambda = 24$ m [37] and processing them through the full simulation chain. The contamination of white kink interactions is evaluated to be 34.6 ± 2.0 in the C1 sample and 3.8 ± 0.4 and 1.5 ± 0.2 in C3 and C5 samples, respectively.

5 Charmed particle production fractions

Since it is not possible to identify the type of charged charmed particles on an event-by-event basis, they are separated using a statistical approach by exploiting the different lifetimes of Λ_c^+ , D^+ and D_s^+ , hence by measuring the flight length and the momentum of the charmed hadrons. The flight length is very precisely measured in the emulsion target. The flight length distributions for the 1-prong and 3-prong events are shown in Fig. 2. The momentum is not directly measured, but it can be estimated exploiting the correlation

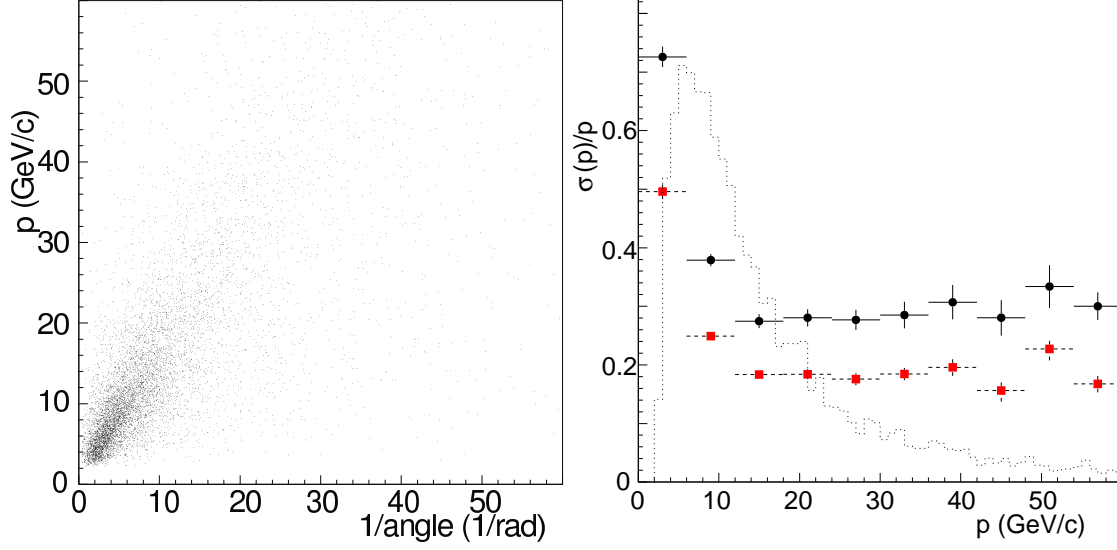


Figure 3: Left: correlation between charm momentum and inverse daughter's opening angle; Right: charm momentum resolution obtained with the Monte Carlo parametrization. Circles indicate 1-prong events, squares 3-prong events. The simulated charm momentum spectrum is superimposed in arbitrary units.

between the momentum and the decay angle of the products [38]. For a given decay mode this correlation is determined by the decay kinematics. Figure 3 shows the correlation between charm momentum and the daughter's inverse opening angle. The charm parent momentum is obtained from the opening angle of the decay products using a parametrization evaluated with simulated events. The resolution obtained with this method is about 25% for 3 prong events and 35% for 1 prong events.

To achieve statistical separation of the different charged charm species, a likelihood function is constructed for each event using the decay lifetime information. Following Ref. [39] the form of the probability function for each event (n) is expressed as the sum of probabilities for the three final state particle hypotheses i ($i = \Lambda_c^+, D^+, D_s^+$). Using the numbers of hadrons of each species, N_i , as the free parameters of the fit, the probability takes the form:

$$P(n) = \frac{\sum_i N_i w_i(n) \epsilon_i[l(n)] \left(\frac{M_i u}{c\tau_i p_i(n)}\right) e^{-\frac{M_i l(n)}{c\tau_i p_i(n)}}}{\sum_i N_i},$$

where $l(n)$ is the measured decay length and $p_i(n)$ is the estimated momentum for the hypothesis i . The efficiencies $\epsilon_i(l)$ are a function of the decay length for each different hadron species i . The mean lifetimes τ_i and the masses of the charmed hadrons M_i are taken from [40]. The weights

$$w_i = \left[\int \frac{M_i u}{c\tau_i p_i} e^{-\frac{l M_i}{c\tau_i p_i}} \epsilon_i(l) dl \right]^{-1}$$

account for the lifetime spectrum deformation due to selection efficiencies. We have introduced u , an arbitrary unit length.

From the probability functions for each event, an extended log-likelihood function is constructed:

$$L = - \sum_n \log P_n - N_{\text{obs}} \log (N_{\Lambda_c^+} + N_{D^+} + N_{D_s^+}) + (N_{\Lambda_c^+} + N_{D^+} + N_{D_s^+})$$

The second and third terms above are the log of the Poisson probability function to observe N_{obs} events given the produced events. The Poisson term incorporates the finite statistics of the experiment. The negative log-likelihood function is then minimized. To be independent of charm topological branching ratios, the one-prong and three-prong samples are fitted separately.

For the one-prong sample, out of 93807 CC events, the result of the fit is

$$N_{\Lambda_c^+}^{1p} = 514 \pm 178 \pm 72 \quad N_{D^+}^{1p} = 980 \pm 192 \pm 50 \quad N_{D_s^+}^{1p} = 449 \pm 235 \pm 27,$$

and for the three-prong sample

$$N_{\Lambda_c^+}^{3p} = 507 \pm 88 \pm 61 \quad N_{D^+}^{3p} = 368 \pm 88 \pm 15 \quad N_{D_s^+}^{3p} = 173 \pm 102 \pm 10,$$

where the first error is the statistical error given by the fit and the second is due to the systematic effect on the efficiencies discussed in the previous section. Given the small statistics, the five-prong sample is included as a correction. This approximation has a negligible effect on the final result owing to the small value of this branching ratio. The relative contributions of charged charm species are:

$$f_{\Lambda_c^+} = (34.1 \pm 7.8)\% \quad f_{D^+} = (44.9 \pm 8.4)\% \quad f_{D_s^+} = (21.0 \pm 8.6)\%.$$

The correlation coefficients are relatively large and similar for the one-prong and three-prong fits. We find $\rho(\Lambda_c^+, D^+) \approx 0.3$, $\rho(\Lambda_c^+, D_s^+) \approx -0.65$, and $\rho(D^+, D_s^+) \approx -0.75$.

6 Topological branching ratios

From the results given in the previous section it is possible to estimate the inclusive topological decay modes for the different charged charm species. In spite of the relatively large errors this information is useful given the fact that, for each charged charm species, the existing measurements cover only half of all decay modes. We find:

$$\begin{aligned} BR(\Lambda_c^+ \rightarrow 3 \text{ prongs}) &= (0.49 \pm 0.15) \\ BR(D^+ \rightarrow 3 \text{ prongs}) &= (0.27 \pm 0.08) \\ BR(D_s^+ \rightarrow 3 \text{ prongs}) &= (0.27 \pm 0.19). \end{aligned} \tag{1}$$

The value of the Λ_c^+ 3-prong branching fraction is 1.5 standard deviations from the one quoted in a previous CHORUS publication [41]. In the present analysis no assumption is made on the other charmed hadron topological branching ratios, while in Ref. [41] a specific assumption had been made. It should also be noted that the decay-recognition efficiencies are significantly different in the analysis of [41] compared to the present analysis. Owing to advances in the automatic pattern recognition it is possible to define larger tolerances on the distance of closest approach of the decay daughter with respect to the primary muon. In addition, in Ref. [41] an equal fraction of QE to DIS Λ_c^+ production was assumed, while in this paper the value of 0.15 ± 0.09 obtained in Ref. [35] was used. The samples in the two analyses are largely independent due to the smaller initial sample available in Ref. [41] and the different cuts applied.

The number of charmed hadrons decaying into 5 charged particles is 22 with a background of 1.5 events. This is too small to fit the different contributions. Assuming that the 5-prong decays are equally distributed

among the three charged charm species and correcting for the efficiency we have $N_{C5} = 42.6 \pm 9.1$. The overall charged charm topological branching fractions are:

$$\begin{aligned} BR(C^+ \rightarrow 1 \text{ prongs}) &= (0.64 \pm 0.10) \\ BR(C^+ \rightarrow 3 \text{ prongs}) &= (0.35 \pm 0.06) \\ BR(C^+ \rightarrow 5 \text{ prongs}) &= (0.014 \pm 0.003). \end{aligned} \quad (2)$$

7 D^0 production cross-section

The cross-section for the production of neutral charmed meson D^0 in neutrino CC interactions has been measured using the same sample of charm candidates [20]. The analysis was based on the sample of D^0 decaying into four charged particles and on the well measured branching ratio $BR(D^0 \rightarrow 4 \text{ prongs})$. By using the same method with the updated value quoted in [40], $BR(D^0 \rightarrow 4 \text{ prongs}) = 0.143 \pm 0.005$, we obtain the value of the cross-section

$$\sigma(\nu_\mu N \rightarrow \mu^- D^0 X) / \sigma(\nu_\mu N \rightarrow \mu^- X) = (2.52 \pm 0.17(\text{stat}) \pm 0.12(\text{syst}))\%. \quad (3)$$

It is important to observe that in Ref. [20] also the decay of D^0 into a fully neutral final state was indirectly measured by subtracting the branching fractions for 2, 4 and 6 prongs from unity. The updated value is

$$BR(D^0 \rightarrow 0 \text{ prongs}) = 0.17 \pm 0.06(\text{stat}) \pm 0.03(\text{syst}). \quad (4)$$

The latter measurements together with the topological branching ratios quoted above have an effect on the determination of the muonic branching ratio of charmed hadrons as reported in Ref. [42]. The updated value is

$$B_\mu = (8.1 \pm 0.9(\text{stat}) \pm 0.2(\text{syst}))\%. \quad (5)$$

This is in good agreement with value of $B_\mu = (9.6 \pm 0.4(\text{stat}) \pm 0.8(\text{syst}))\%$ obtained in the CHORUS dimuon event analysis [11].

8 Charm cross-sections

By using the fitted quantities of the one prong and three prong samples and the corrected number of 5-prong events, a relative cross-section

$$\sigma(\nu_\mu N \rightarrow \mu^- C^+ X) / \sigma(\nu_\mu N \rightarrow \mu^- X) = (3.23 \pm 0.27(\text{stat}) \pm 0.21(\text{syst}))\% \quad (6)$$

is obtained for the charged charm production rate in charged-current interactions. Forcing the Λ_c^+ 1-prong to 3-prong ratio to be that of Ref. [41] hardly affects the total charm cross-section (by about one-quarter of the systematic error).

Including the result obtained for the neutral charmed meson D^0 given in the previous section, the relative inclusive charm production rate in charged-current interactions is

$$\sigma(\nu_\mu N \rightarrow \mu^- C X) / \sigma(\nu_\mu N \rightarrow \mu^- X) = (5.75 \pm 0.32(\text{stat}) \pm 0.30(\text{syst}))\% \quad (7)$$

with a relative contribution of the charm species:

$$f_{D^0} = (43.7 \pm 4.5)\% \quad f_{\Lambda_c^+} = (19.2 \pm 4.2)\% \quad f_{D^+} = (25.3 \pm 4.4)\% \quad f_{D_s^+} = (11.8 \pm 4.7)\%.$$

In Ref. [43] we reported that in anti-neutrino CC interactions $\sigma(\bar{\nu}_\mu N \rightarrow \mu^+ \bar{C} X) / \sigma(\bar{\nu}_\mu N \rightarrow \mu^+ X) = (5.0_{-0.9}^{+1.4}(\text{stat}) \pm 0.7(\text{syst}))\%$. The value is similar to what we find for neutrino interactions as expected since both total CC cross-section and charm production are about half in this case.

The energy dependence of the relative charm production cross-section is obtained by estimating the energy of the interacting neutrino on an event-by-event basis. A good estimate is the sum of the energy of the primary muon and the total energy deposition in the calorimeter corrected for the energy deposited by the muon and for the unmeasured energy loss of hadrons in the material upstream of the calorimeter. The unmeasured part is mainly due to the absorption in the emulsion stacks and corrected to the measured vertex position. The resolution of the calorimeter energy measurement is $\sigma(E)/E = (0.323 \pm 0.024) / \sqrt{E/\text{GeV}} + (0.014 \pm 0.007)$ [16]. The momentum resolution varies from $\sim 15\%$ [16] in the 12–28 GeV/c interval to $\sim 19\%$ [16] at about 70 GeV/c, as measured with test-beam muons. Given the relatively small size of the energy bins, the average neutrino energy is very similar for charm production events and CC events within the same bin, and no correction is necessary. The efficiency is calculated by weighting the energy-dependent and decay topology-dependent efficiencies with the measured branching ratios as reported above.

The energy dependence of backgrounds is assumed to be the same as the one of charged current neutrino events. The differential cross-section measurement is normalized to the total neutrino–nucleon cross-section and thus is not affected by the uncertainties between the beam simulation and the beam flux measurement. The measurement of the charm production rate relative to the CC interaction rate is shown as function of neutrino energy and compared with the measurement from E531 [15] in Figure 4. Good agreement with an improved precision with respect to E531 measurement is shown. Very good agreement is found with respect to the dimuon cross-section measured with the CHORUS electronic detector by scaling the dimuon results for the muonic charm decay fraction quoted in this paper.

The energy dependence for charged and neutral charm is reported separately in Figure 5. A very similar energy behaviour is shown except for the low energy region where the contribution of quasi-elastic production of Λ_c^+ may account for the difference [35].

9 Acknowledgements

We gratefully acknowledge the help and support of the neutrino-beam staff and of the numerous technical collaborators who contributed to the detector construction, operation, emulsion pouring, development, and scanning. The experiment was made possible by grants from the Institut Interuniversitaire des Sciences Nucléaires and the Interuniversitair Instituut voor Kernwetenschappen (Belgium); the Israel Science Foundation (Grant 328/94) and the Technion Vice President Fund for the Promotion of Research (Israel); CERN (Geneva, Switzerland); the German Bundesministerium für Bildung und Forschung (Germany); the Institute of Theoretical and Experimental Physics (Moscow, Russia); the Istituto Nazionale di Fisica Nucleare (Italy); the Promotion and Mutual Aid Corporation for Private Schools of Japan and Japan Society for the Promotion of Science (Japan); Korea Research Foundation Grant (KRF-2003-005-C00014) (Republic of Korea); the Foundation for Fundamental Research on Matter FOM and the National Scientific Research Organization NWO (The Netherlands); and the Scientific, and Technical Research Council of Turkey (Turkey). We gratefully acknowledge their support.

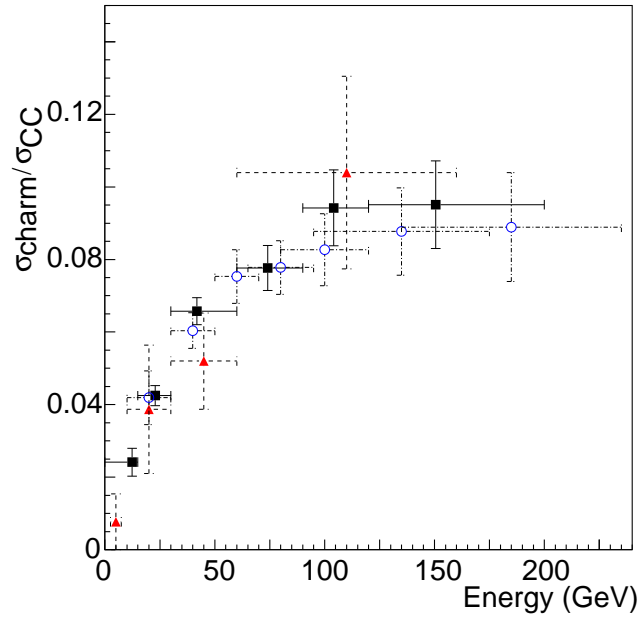


Figure 4: Energy dependence of the relative inclusive charm production cross-section ratio. The squares show the measurements reported here, the points marked with triangles the E531 result. The circles represent the dimuon cross-section measured in Ref. [11] scaled for the muonic branching ratio quoted in this paper.

References

- [1] J. E. Augustin *et al.*, *Phys. Rev. Lett.* **33** (1974) 1406.
- [2] J. J. Aubert *et al.*, *Phys. Rev. Lett.* **33** (1974) 1404.
- [3] K. Niu, E. Mikumo, Y. Maeda, *Prog. Theor. Phys.* **46** (1971) 1644.
- [4] R. Acquafredda *et al.*, *JINST* **4**:P04018 (2009).
- [5] J.J. Gomez-Cadenas *et al.*, "Physics opportunities at Neutrino factories", *Ann. Rev. Nucl. Part. Sci.* **52** (2002) 253.
- [6] H. Abramowicz *et al.*, CDHS Collaboration, *Z. Phys.* **C15** (1982) 19.
- [7] S.A. Rabinowitz *et al.*, CCFR Collaboration, *Phys. Rev. Lett.* **70** (1993) 134.
- [8] M. Jonker *et al.*, CHARM Collaboration, *Phys. Lett.* **B107** (1981) 241.
- [9] P. Vilain *et al.*, CHARM II Collaboration, *Eur. Phys. J.* **C11** (1999) 19.
- [10] M. Goncharov *et al.*, NuTeV Collaboration, *Phys. Rev.* **D64** (2001) 112006.
- [11] A. Kayis-Topaksu *et al.*, CHORUS Collaboration, *Nucl. Phys.* **B798** (2008) 1.
- [12] A. E. Asratian *et al.*, *Z. Phys.* **C68** (1995) 43.

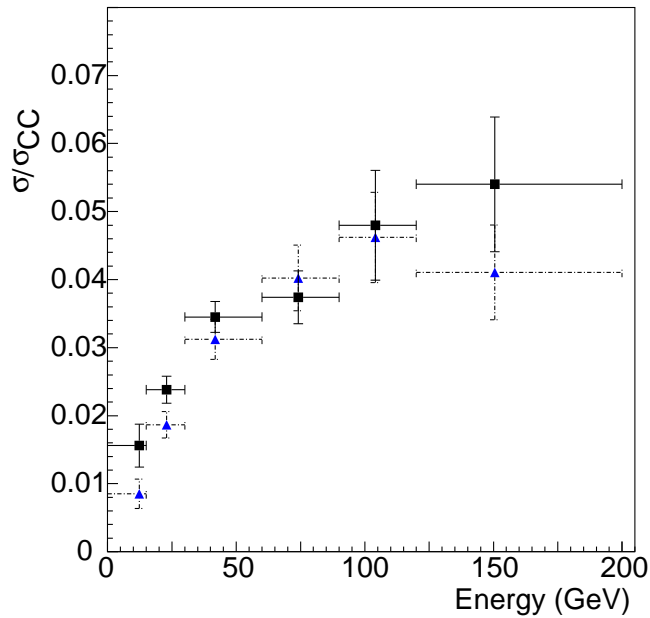


Figure 5: Energy dependence for charged (squares) and neutral (triangles) charm cross-section ratio relative to the CC cross-section.

- [13] P. Astier *et al.*, NOMAD Collaboration, *Phys. Lett.* **B486** (2000) 35.
- [14] G. Onengut *et al.*, CHORUS Collaboration, *Phys. Lett.* **B614** (2005) 155.
- [15] N. Ushida, *et al.*, E531 Collaboration, *Phys. Lett.* **B206** (1988) 375.
- [16] E. Eskut, *et al.*, CHORUS Collaboration, *Nucl. Instrum. and Methods* **A401** (1997) 7.
- [17] S. Aoki *et al.*, *Nucl. Instrum. and Methods* **B51** (1990) 466.
- [18] T. Nakano. Ph.D. thesis, Nagoya University, Japan, 1997.
- [19] E. H. M. Heijne, CERN Yellow Report 83-06 (1983).
- [20] G. Onengut *et al.*, CHORUS Collaboration, *Phys. Lett.* **B613** (2005) 105.
- [21] M.G. van Beuzekom, *et al.*, CHORUS Collaboration, *Nucl. Instrum. and Methods* **A427** (1999) 587.
- [22] A. M. Güler, Ph.D. thesis, Middle East Technical University, Ankara, Turkey (2000).
- [23] B. Van de Vyver, Ph.D. thesis, Vrije Universiteit Brussel, Brussels, Belgium, 2002. CERN-THESIS-2002-024.
- [24] N. Nonaka, Ph.D. thesis, Nagoya University, Japan (2002).
- [25] I. Tsukerman, CHORUS Collaboration, MC Generators in CHORUS, *Nucl. Phys. Proc. Suppl.* **112** (2002) 177.
- [26] S. Sorrentino, Diploma Thesis, Naples University, Italy (1995).

- [27] GEANT 3.21, CERN program library long write up W5013.
- [28] A. Fassò *et al.*, SARE-3 Workshop, KEK Report Proceedings 97-5 (1997) 32.
- [29] P. Zucchelli, Ph.D. thesis, Università di Ferrara, Italy (1995).
- [30] G. Ingelman, *Preprint TSL/ISV 92-0065*, Uppsala University, Sweden (1992).
- [31] T. Sjöstrand, *Comput. Phys. Commun.* **82** (1994) 74.
- [32] S. Ricciardi, Ph.D. thesis, Università di Ferrara, Italy (1996).
- [33] F. Di Capua, Ph.D. thesis, Università di Napoli, Italy (2003).
- [34] O. Melzer, Diploma thesis, Westfälische Wilhelms-Universität, Münster, Germany (1997).
- [35] A. Kayis-Topaksu *et al.*, CHORUS Collaboration, *Phys. Lett.* **B575** (2003) 198.
- [36] G. De Lellis *et al.*, *Phys. Lett.* **B550** (2002) 16.
- [37] A. Satta, Ph.D. thesis, Università La Sapienza di Roma, Italy (2001).
- [38] S. Petrerá and G. Romano, *Nucl. Instrum. and Meth* **174** (1980) 61.
- [39] T. Bolton, arXiv:hep-ex/9708014.
- [40] Particle Data Group, *J. of Physics* **G37** (2010) 075021.
- [41] A. Kayis-Topaksu *et al.*, CHORUS Collaboration, *Phys. Lett.* **B555** (2003) 156.
- [42] A. Kayis-Topaksu *et al.*, CHORUS Collaboration, *Phys. Lett.* **B626** (2005) 24.
- [43] G. Onengut *et al.*, CHORUS Collaboration, *Phys. Lett.* **B604** (2004) 145.